www.czasopisma.pan.pl PAN www.journals.pan.pl
Opto-Electronics Review 27 (2019) 1–9

Contents lists available at ScienceDirect

Opto-Electronics Review

journal homepage: http://www.journals.elsevier.com/opto-electronics review

Numerical investigation of a broadband coherent supercontinuum generation in $Ga_8Sb_{32}S_{60}$ chalcogenide photonic crystal fiber with all-normal dispersion

A. Medjouri [a,*], D. Abed [b], Z. Becer [a]

[a] LEVRES Laboratory, Faculty of Exact Sciences, University of Echahid Hamma Lakhdar EL Oued, BP 789, El Oued, 39000, Algeria
[b] Department of Electronics and Telecommunications, Faculty of Sciences and Technology, University of 8 mai 1945 Guelma, 24000, Guelma, Algeria

ARTICLE INFO

Article history:
Received 28 July 2018
Received in revised form 4 January 2019
Accepted 7 January 2019
Available online 21 January 2019

Keywords:
Nonlinear optics
$Ga_8Sb_{32}S_{60}$ chalcogenide glass
Supercontinuum generation
FDFD method
Photonic crystal fiber

ABSTRACT

All normal dispersion (ANDi) and highly nonlinear chalcogenide glass photonic crystal fiber (PCF) is proposed and numerically investigated for a broad, coherent and ultra-flat mid-infrared supercontinuum generation. The proposed PCF consists of a solid core made of $Ga_8Sb_{32}S_{60}$ glass surrounded by seven rings of air holes arranged in a triangular lattice. We show by employing the finite difference frequency domain (FDFD) method that the $Ga_8Sb_{32}S_{60}$ PCF dispersion properties can be engineered by carefully adjusting the air holes diameter in the cladding region and ANDi regime is achieved over the entire range of wavelengths with a zero chromatic dispersion around 4.5 μm. Moreover, we demonstrate that injecting 50 fs width and 20 kW peak power laser pulses (corresponding to a pulse energy of 1.06 nJ) at a pump wavelength of 4.5 μm into a 1 cm long ANDi $Ga_8Sb_{32}S_{60}$ PCF generates a broad, flat-top and perfectly coherent SC spectrum extending from 1.65 μm to 9.24 μm at the 20 dB spectral flatness. These results make the proposed $Ga_8Sb_{32}S_{60}$ PCF an excellent candidate for various important mid-infrared region applications including mid-infrared spectroscopy, medical imaging, optical coherence tomography and materials characterization.

1. Introduction

Supercontinuum (SC) generation refers to the substantial spectral broadening obtained by using ultrafast laser pulses propagating in nonlinear medium [1]. Since the first experimental observation of the white light continuum in a borosilicate glass sample in the beginning of the 1970s [2], SC has become a significant scientific success and has found numerous applications including ultrafast laser spectroscopy, frequency comb generation, optical communications, optical coherence tomography (OCT), metrology and nonlinear optical pulse compression [3]. Under femtosecond pumping, the generation of spectrally continuous radiation results from the contribution of several linear and nonlinear processes and is strongly related to the dispersion profile exhibited by the optical waveguide [4]. When pumping in the anomalous regime of dispersion, soliton dynamics, dispersive wave generation and Raman self-frequency shifting are responsible for the SC process [5]. The generated spectra are ultra-wide, as a result of appearing of new optical pulses created from the fission of the fundamental Soliton. Nevertheless, the SC spectra are not completely coherent because of their sensitivity to the noise amplification and, hence, shot-to-shot fluctuations [6]. On the other hand, achieving SC generation by pumping optical pulses at the normal dispersion regime can be triggered by self phase modulation (SPM) and the pulse spectrum extends toward longer wavelengths because of the optical wave breaking (OWB) mechanism. The generated SC spectra are narrow compared to that produced with the anomalous dispersion regime, but exhibit smooth profile and high degree of coherence [7].

Dynamics of a supercontinuum formation results from the interplay between a plethora of linear and nonlinear optical effects which come together to produce the spectral broadening of laser pulses, commonly over short propagation lengths [8]. Even though bulk media provide some interesting features related to the strong spatiotemporal coupling, guiding medium such as optical fibers is much more interesting as their optical properties can be adjusted, notably with the invention of photonic crystal fibers (PCFs) [9]. The main advantage of PCF resides in its versatility in terms of morphology, application and glass used for its fabrication [10]. Therefore, PCFs geometries can be optimized to, simultaneously, engineer the dispersion properties and increase the Kerr nonlinearity [11].

Chalcogenide (ChG) glasses are compound that contain at least one of the chalcogen elements S, Se, and Te combined with the other elements such as Sb, Ge, As, Ga, etc. [12,13]. ChG glasses are of great interest due to the possibility of producing glass systems with large

* Corresponding author.
E-mail address: medjouri-abdelkader@univ-eloued.dz (A. Medjouri).

https://doi.org/10.1016/j.opelre.2019.01.003
1230-3402/

composition space and good resistance to crystallization which yield to achieve excellent optical properties such as high refractive indices, high Kerr nonlinearities, and broad transparency window extending from near-infrared to mid-infrared wavelengths [14,15]. Owing to these excellent optical properties, ChG glasses have been extensively employed to design mid-infrared SC laser sources based on PCF exhibiting all-normal chromatic dispersion (ANDi) profile [12]. Yan *et al.* numerically investigated coherent SC generation extending from 2 to 5 μm by pumping 50 fs duration 1 kW peak power laser pulses in As_2S_3 ChG glass PCF [16]. The authors have optimized the PCF dispersion profile by controlling the air hole diameters of inner layers. By using a similar approach, T.S. Saini *et al.* reported SC spectra spanning 1.9–10 μm by pumping at 4.5 μm, 50 fs width 0.7 kW peak power laser pulses in As_2Se_3 ChG glass triangular-core PCF [17]. Furthermore, Diouf *et al.* reported a coherent super-flat SC source in hexagonal lattice PCF made of $As_{38.8}Se_{61.2}$ ChG [18]. Dispersion and nonlinear parameters of the proposed PCF are engineered by adjusting the air holes diameter in the aim to achieve both ANDi regime and high Kerr nonlinearities. They have numerically shown that coherent SC spectrum extending from 2.9 to 4.575 μm at a 3 dB spectral flatness level can be achieved by launching a 0.05 nJ energy laser pulses pumped at a central wavelength of 3.7 μm into a 5 cm ANDi PCF length. A. Ben Salem *et al.* reported SC generation in a kind of hybrid PCF composed of As_2S_5 ChG glass and borosilicate [19]. The authors have shown that coherent and ultra-flat SC spectra spanning from 1 to 5 μm can be obtained by injecting at 2.5 μm, 50 fs pulses with 28.16 kW peak power through 4 mm PCF length. Mid-infrared SC extending from 1.5 to 12.2 μm has been, also, reported in $AsSe_2$ ChG based PCF by Diouf *et al.* [20]. The authors have shown that such broadband spectra can be obtained by pumping 100 fs pulses with a peak power of 11.44 kW at 3.5 μm. Karim *et al.* used a hexagonal lattice PCF made using $Ge_{11.5}As_{24}Se_{64.5}$ glass in the aim to generate super-flat and broadband SC in ANDi regime [21]. The results, obtained via numerical simulations, indicate that by pumping at 3.1 μm laser pulses with a 50 fs width and a 5 kW peak power, a SC extended up to 6 μm can be obtained. Moreover, Karim *et al.* reported a coherent SC generation spanning beyond 15 μm with a 1 cm all-chalcogenide dispersion-engineered triangular core fiber (TCF) by using a pump at 4 μm with a peak power of 5 kW [22]. The proposed TCF is composed of a solid core of $Ge_{11.5}As_{24}Se_{64.5}$ ChG glass surrounded by a cladding made of $Ge_{11.5}As_{24}S_{64.5}$ ChG glass.

Recently, a novel Ga–Sb–S ChG glass system has been proposed for mid-infrared applications [23]. The Ga–Sb–S based ChG glass has excellent optical properties such as broad transparency wavelength range extending from 0.8 to 14 μm, high linear refractive index laying in the range of 2.62–2.70, high third-order nonlinear refractive index up to 12.4×10^{-14} cm^2/W at the wavelength of 1.55 μm, large solubility and low phonon energy when doping with rare earth [23]. Besides, Ga-based glasses combined with heavy metals exhibit smaller multi-photon spectra which is suitable for the design of lasers and other photonic applications [24]. Boruah *et al.* proposed and numerically investigated optical properties of low bend loss PCF based on $Ga_8Sb_{32}S_{60}$ ChG glass for mid-infrared nonlinear applications [25]. The proposed structure is found to be highly nonlinear and insensitive to microbending which makes it an excellent candidate for nonlinear applications such as SC generation. Ga–Sb–S ChG glass system has been, also, considered to design a rib waveguide for an on-chip mid-infrared SC generation [24]. The waveguide geometry consists of a $Ga_8Sb_{32}S_{60}$ ChG glass core surrounded by a layer of MgF_2 glass which act as an upper and lower cladding material. By pumping at 2.8 μm optical pulses with a 497 fs duration and a 6.4 kW peak power, mid-infrared SC spanning the spectral band extending from 1 to 9.7 μm can be, successfully, achieved [24]. However, the generated spectra are not smooth because of the anomalous dispersion regime exhibited by the proposed rib waveguide. To overcome this critical limitation, ANDi regime can be achieved in PCF through a proper adjustment of its air holes diameter.

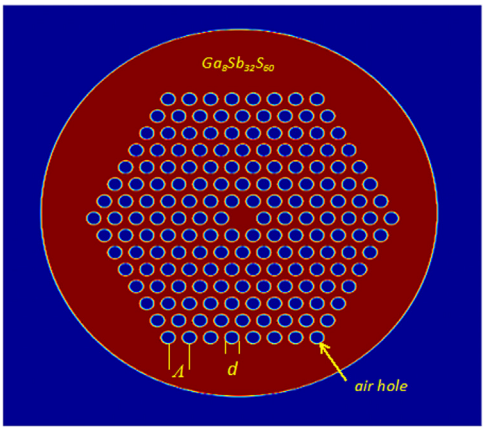

Fig. 1. Cross sectional view of the proposed $Ga_8Sb_{32}S_{60}$ ChG glass PCF.

In this work, we report on a numerical modelling of a mid-infrared SC generation in a dispersion engineered hexagonal lattice PCF with a background material made of $Ga_8Sb_{32}S_{60}$ ChG glass. To achieve a broadband, coherent and flat-top SC in the mid-infrared region, the proposed $Ga_8Sb_{32}S_{60}$ PCF is specifically designed with ANDi profile and nearly-zero chromatic dispersion wavelength in the mid-infrared region. This characteristics can be fulfilled with appropriately controlling the cladding air holes diameter. For that purpose, the finite-difference frequency-domain (FDFD) method is employed to compute the PCF linear and nonlinear properties such as chromatic dispersion, field mode area and Kerr nonlinear coefficient. The spectral broadening occurring due to the propagation of high peak power and femtosecond laser pulses inside the proposed PCF is simulated by solving the generalized nonlinear schrödinger equation (GNLSE). Furthermore, the influence of pulses' characteristics and the seeded noise on the generated SC bandwidth and coherence is, respectively, investigated.

2. Theory

2.1. Design and parameters computation of the $Ga_8Sb_{32}S_{60}$ PCF

Figure 1 depicts the cross section of our proposed PCF. The structure is formed by a solid core made of $Ga_8Sb_{32}S_{60}$ ChG glass surrounded by seven rings of air holes arranged in a triangular lattice and running along the PCF length. The number of rings has been chosen to prevent the confinement loss which arises due to the optical tunnel effect. The air holes pitch and diameter are Λ and d, respectively. The refractive index of $Ga_8Sb_{32}S_{60}$ ChG glass is calculated by using the Sellmeier dispersive model as [25]:

$$n = \sqrt{1 + \frac{a_1\lambda^2}{\lambda^2 - b_1^2} + \frac{a_2\lambda^2}{\lambda^2 - b_2^2}}. \quad (1)$$

Where: $a_1 = 6.2563$, $b_1 = 0.3425$ μm, $a_2 = 2.9444$ and $b_2 = 34.28$ μm.

In order to compute the fundamental mode effective index and find the corresponding optical field distribution, the finite-difference frequency-domain (FDFD) method has been used. After applying the PML boundary condition, the Maxwell's equations for the electric field E and magnetic field H are given by [26]:

$$\begin{cases} ik_0 s\varepsilon_r E = \nabla \times H \\ -ik_0 s\mu_r H = \nabla \times E \end{cases} \quad (2)$$

$$s = \begin{bmatrix} s_y/s_x & 0 & 0 \\ 0 & s_x/s_y & 0 \\ 0 & 0 & s_y s_x \end{bmatrix}. \quad (3)$$

Where: $s_x = 1 - \sigma_x/(i\omega\varepsilon_0)$ and $s_y = 1 - \sigma_y/(i\omega\varepsilon_0)$.

k_0 is the free space number, ε_r is the medium relative permittivity, μ_r is the medium relative permeability, σ is the conductivity profile and ω is the angular frequency. Once an adequate meshing is introduced to the structure, the Maxwell's equations system is converted into a matrix eigenvalue problem. For a given excitation wavelength, a sparse matrix method is used to compute the mode effective refractive index n_{eff} and its optical field profile [27].

The chromatic dispersion is a key parameter in the propagation of short optical pulses and their nonlinear interactions in optical fibers [4]. The PCF chromatic dispersion coefficient is evaluated from the fundamental mode effective index as follows:

$$D(\lambda) = -\frac{\lambda}{c}\frac{d^2 n_{eff}}{d\lambda^2}. \quad (4)$$

Where λ and c are the wavelength and the speed of light, respectively.

The field effective area of the propagating mode plays a crucial role in designing PCFs. It gives a measurement of the light transmitting area regarding the PCF nonlinear response. It can be calculated using [28]:

$$A_{eff} = \frac{\left(\iint |E^2| \, dxdy\right)^2}{\iint |E|^4 \, dxdy}. \quad (5)$$

Where E denotes now the amplitude of the transverse electric field that propagates within the PCF.

The PCF Kerr nonlinearity coefficient is defined as [5]:

$$\gamma = \frac{n_2 \omega_0}{c A_{eff}}. \quad (6)$$

Where $n_2 = 12.4 \times 10^{-14}\, cm^2/W$ at 1.55 μm for $Ga_8Sb_{32}S_{60}$ ChG glass [23].

2.2. Modelling of nonlinear pulse propagation in PCFs

Ultra-court pulse propagation and SC generation in PCFs can be modelled by the generalized nonlinear schrödinger equation (GNLSE) [5]. This propagation's equation describes the pulse evolution inside an optical fiber with the mutually combined effects of chromatic dispersion and the various nonlinear processes. Its expression is given by:

$$\frac{\partial A}{\partial z} + \frac{\alpha}{2}A - \sum_{k\geq 2}\frac{I^{k+1}}{k!}\beta_k \frac{\partial^k A}{\partial T^k} = i\gamma\left(1 + \frac{i}{\omega_0}\frac{\partial}{\partial T}\right)$$
$$\left(A(z,T)\int_{-\infty}^{\infty} R(T') \times \left|A(z, T-T')\right|^2 dT'\right). \quad (7)$$

$A(z,T)$ is the temporal envelope of the pulse electric field, α is the propagation loss coefficient, β_k is the k^{th} Taylor series expansion coefficient of the propagation constant $\beta(\omega)$ computed at the center carrier frequency ω_0 of the pumping pulse, γ is the Kerr nonlinearity coefficient, $R(T)$ is the nonlinear response function, that contains both instantaneous electronic (Kerr effect) and delayed (Raman scattering) contributions. Its expression is given by Ref. 5:

$$R(t) = (1 - f_R)\delta(t) + f_R h_R(t). \quad (8)$$

$\delta(t)$ is the Dirac delta function that represents the instantaneous electronic response, $h_R(t)$ is the Raman response function and f_R represents the Raman fractional contribution to the overall nonlinear response. Given that, the $Ga_8Sb_{32}S_{60}$ ChG glass Raman response and fractional contribution are unknown, we have employed those of the As_2Se_3 ChG glass [24]. Accordingly, the value of f_R is set to be 0.115 and the Raman response is given by the following expression [17]:

$$h_R(t) = \frac{\tau_1^2 + \tau_2^2}{\tau_1 \tau_2^2} exp\left(\frac{-t}{\tau_2}\right) sin\left(\frac{t}{\tau_1}\right)\Theta(t). \quad (9)$$

This single Lorentzian model is characterized by two parameters τ_1 and τ_2 which are appropriately adjusted to provide an excellent fit to the real Raman gain spectrum [29]. τ_1 is related to the phonon frequency and τ_2 is related to the network attenuation of vibrating atoms [30]. Their values are set to be of 23.1 fs and 195 fs, respectively [17].

Finally, the statistical properties of the generated SC are investigated. Aiming to analyze their sensitivity to the input noise present on the pump pulses. Coherence of SC sources refers to a measure of correlations among their spectral intensities and is required to characterize ultrafast or rarely occurring phenomena [31]. The analysis can be performed by calculating the modulus of the first-order degree of coherence described as the ratio of the mean spectral field squared to the mean spectral intensity as following [32]:

$$|g_{12}(\omega)| = \frac{|<E(\omega)>|^2}{<|E(\omega)|^2>}. \quad (10)$$

Where $E(\omega)$ is the output pulse spectrum. The degree of coherence is calculated considering an ensemble average over a large number of independent realizations of the generated SC spectra. The input pulse noise is seeded into each of these simulations based on the one photon per mode model [33]. The spectral amplitude of the input noise $A(\omega)$ can be expressed as [34]:

$$A(\omega) = \sqrt{\frac{\hbar\omega}{T_{span}}} exp(i2\pi\varphi(\omega)). \quad (11)$$

Where $\hbar$ is the reduced Planck constant, ω is the angular pulsation, T_{span} is the temporal window employed for the numerical simulations and $\varphi(\omega)$ is a randomly generated phase, uniformly distributed in the interval $[0, 2\pi]$. Besides, $|g_{12}(\omega)|$ is lying in the interval [0–1], with a value of 1 indicating perfect coherence [5].

3. Numerical results

3.1. Dispersion engineering of the proposed PCF

As stated previously, our target is to design $Ga_8Sb_{32}S_{60}$ ChG glass based hexagonal lattice PCF exhibiting ANDi regime so that the resulting SC is flat and coherent over a broad spectral range. For this purpose, the geometrical parameters of the proposed PCF are suitably adjusted. In fact, the material dispersion of the background glass is a fundamental limit when engineering the PCF chromatic [35]. Figure 2 depicts the material dispersion of $Ga_8Sb_{32}S_{60}$ ChG glass derived from Eq. (1). As it can be seen, the glass exhibits both normal and anomalous dispersion with a zero dispersion wavelength at 5.25 μm. Through a careful adjusting of the lattice pitch and the air holes diameter, the material dispersion can be adjusted by waveguide dispersion and ANDi regime can be, then, achieved. We optimize the proposed PCF structure considering a constant pitch Λ and different values of air holes diameter. Figure 3 depicts the evolution of the fundamental mode chromatic dispersion with wavelengths for $\Lambda = 2.5\,\mu m$ and d varying from 0.6 μm to 1.2 μm with step of 0.2 μm. As it can be observed, the total chromatic dispersion profile is strongly affected by the value of the air filling fraction. When d/Λ increases, the dispersion curve increases too and a maximum value obtained around the wavelength of 4.5 μm. Besides, ANDi regime can be achieved with a peak close to the zero

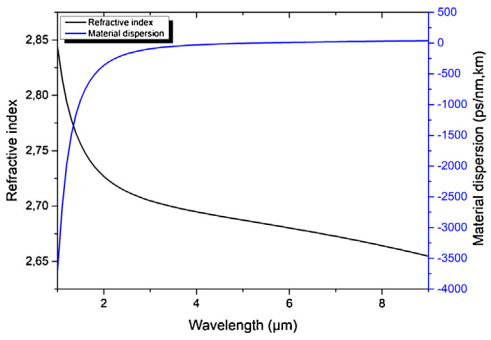

Fig. 2. Refractive index and corresponding material dispersion versus wavelength of the $Ga_8Sb_{32}S_{60}$ ChG glass.

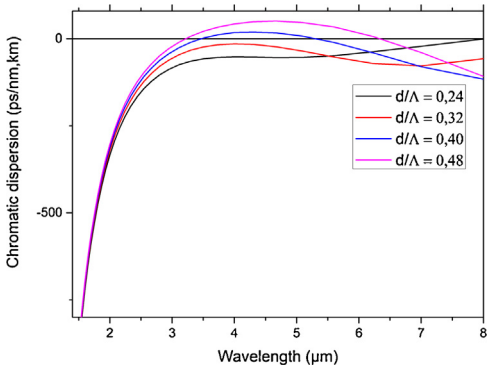

Fig. 3. Variation of the chromatic dispersion with wavelengths for $\Lambda = 2.5\,\mu m$ and d varying from 0.6 μm to 1.2 μm with step of 0.2.

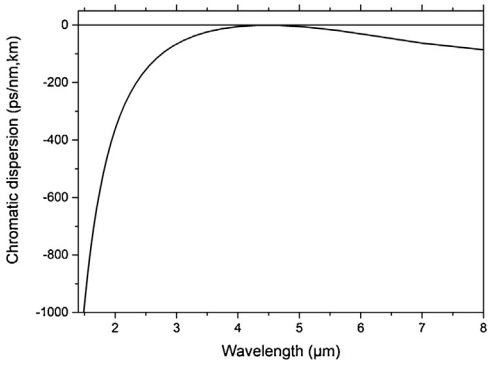

Fig. 4. Variation of the chromatic dispersion with wavelengths for d/ $\Lambda = 0.352$.

for d/Λ laying between 0.32 and 0.40. Further numerical investigations have shown that such required dispersion profile can be ensured with $d/\Lambda = 0.352$, corresponding to an air hole diameter of $d = 0.88\,\mu m$. As depicted in Fig. 4, the PCF design with optimized air holes diameter exhibits a negative dispersion over the entire spectral range with zero dispersion wavelength around 4.5 μm. Finally, we have calculated the effective field mode area and the corresponding Kerr nonlinearity and their variations with wavelengths are depicted in Fig. 5. By using the Miller' rule, the nonlinear refractive index of the $Ga_8Sb_{32}S_{60}$ ChG glass has been reduced to $n_2 = 10.6 \times 10^{-14}\,cm^2/W$, corresponding to the central wavelength 4.5 μm [36]. Simulations results show that the proposed $Ga_8Sb_{32}S_{60}$ PCF exhibits extreme high nonlinearity over the whole spectral range. Moreover, the effective field mode area and the corresponding Kerr nonlinear coefficient for the wavelength of 4.5 μm have been found to be of 15.23 μm^2 and 970 $w^{-1}\,km^{-1}$, respectively.

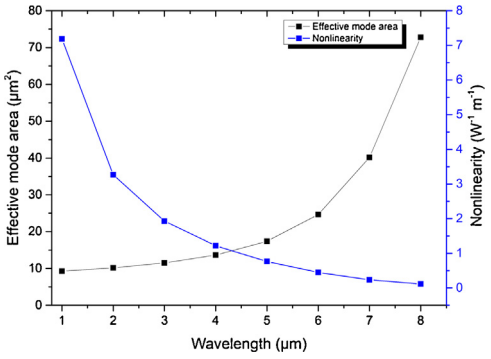

Fig. 5. Variation of the effective mode area and the corresponding nonlinear coefficient with wavelength for d/ $\Lambda = 0.352$.

Table 1
Taylor series expansion coefficients of the propagation constant.

Coefficient	Value
β_2	0.2121 ps^2/km
β_3	−0.0027 ps^3/km
β_4	3.5188×10^{-05} ps^4/km
β_5	-1.8685×10^{-07} ps^5/km
β_6	5.7195×10^{-10} ps^6/km
β_7	-7.8881×10^{-13} ps^7/km

3.2. Simulation of mid-infrared SC in the proposed PCF

For studying SC generation in our proposed PCF with the optimized design, we numerically solve the GNLSE equation given by Eq. (7). Optical pulses propagating within the $Ga_8Sb_{32}S_{60}$ PCF core are modelled by a chirpless Gaussian pulse given by $A(0,t) = \sqrt{P_0} exp\left(-t^2/2T_0^2\right)$ where, T_0 is the pulse duration and P_0 is the peak power. Aiming to generate broad SC, laser pulses are pumped at 4.5 μm, corresponding to the zero chromatic dispersion wavelength. A possible light source for these pulses is based on phase-matched difference-frequency mixing (DFM) in Gallium Selenide (GaSe) crystal of near-infrared signal and idler pulses obtained from a parametric system [37]. The light source is capable of providing optical pulses with μ-joule energy level in the mid-infrared wavelengths range extending from 3 to 20 μm with very short durations of 50 fs at the wavelength of 5 μm. In order to accurately model the dispersion variation over a large spectral bandwidth, the Taylor series expansion coefficients up to the 7th order of the propagation constant have been computed around the center carrier frequency and their corresponding values are given in Table 1. The propagation loss is neglected from Eq. (7) since pulse propagation is considered in only few millimeters PCF length piece.

Firstly, and aiming to give a simple explanation of SC formation mechanisms in the proposed $Ga_8Sb_{32}S_{60}$ PCF, we consider the injection of a Gaussian pulse with a total energy of 0.53 nJ, corresponding to FWHM and a peak power of 100 fs and 5 kW, respectively. Accordingly, the dispersion length L_D, the nonlinear length L_{NL} and the soliton order N can be computed as following: $L_D = T_0^2/\left|\beta_2\right| = 0.047$ m, $L_{NL} = 1/(\gamma P_0) = 20.60 \times 10^{-5}$ m and $N = \sqrt{L_D/L_{NL}} = 15$, respectively. Figure 6 depicts the pulse temporal and spectral evolution over the propagation distance. In the first few millimeters, the SC process is initiated by the SPM and the pulse spectrum extends symmetrically toward shorter and longer wavelengths. Furthermore, the SC spectrum begin to broaden asymmetrically because of the OWB effect. It arises on the pulse leading and trailing edges where the spectrum sidebands are obtained from mixing the overlapping frequency components generated by the SPM [38]. Consequently, OWB is responsible for the creation of the extreme frequencies on both sides of the pulse spec-

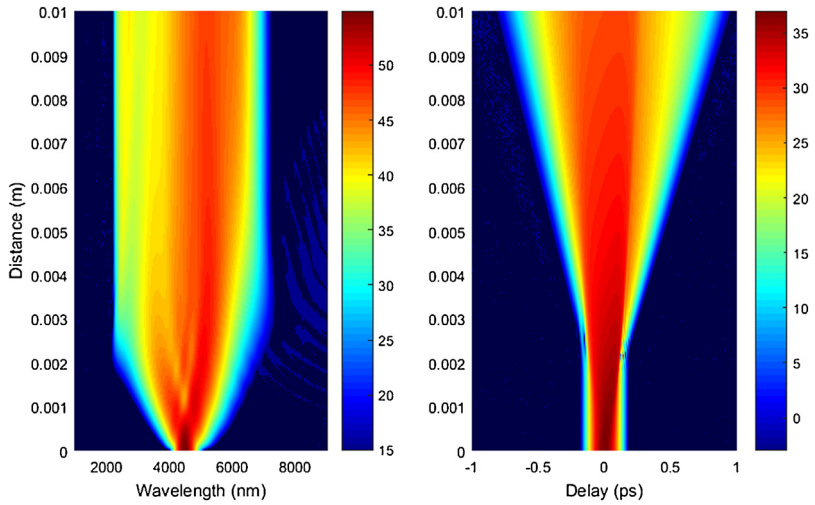

Fig. 6. Gaussian pulse spectral and temporal evolution over 1 cm PCF length where the peak power and FWHM are 5 kW and 100 fs, respectively.

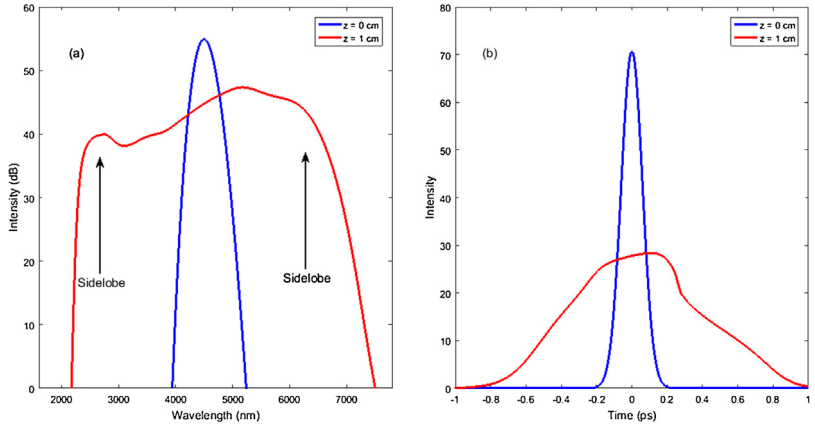

Fig. 7. Pulse spectral (a) and temporal (b) profiles at the input and after z = 1 cm of propagation.

trum and for the uniform spectral and temporal profiles of the pulse spectrum at the PCF output [1]. Figure 7 shows the pulse temporal and spectral profiles at the PCF input and after 1 cm of propagation length. The propagation length where the OWB arises is given by [39]:

$$z = \frac{L_D}{\sqrt{4e^{-1.5}N^2 - 1}} \tag{12}$$

Accordingly, the OWB starts to occur at the distance of 3.3 mm. Figure 8 shows the pulse temporal profile at the input and after 3.3 mm of propagation and the spectrogram of the output pulse. Upon further propagation, the pulse spectrum extends on both sides by transferring energy from its center wavelengths to the new generated frequency band. Sight to enhance the generated SC bandwidth, we have studied the impact of the pumped pulses initial conditions. Firstly, the impact of the pulse peak power is investigated. Numerical simulations are conducted with a 100 fs pulse duration with a peak power of 5 kW, 10 kW, 15 kW and 20 kW, respectively. As it can be seen from Fig. 9, the output pulse spectrum width increases with the initial peak power. Besides, smooth SC spectra extending to the mid infrared region and spanning 6.9 μm in the range from 1.7 μm to 8.6 μm at 20 dB is successfully obtained for a peak power of 20 kW. The effect of the initial pulse duration on the output spectrum bandwidth is, then, studied. We consider an initially injected pulse with a peak power of 20 kW and various FWHM durations. Figure 10 depicts the output pulse spectrum after propagation over PCF length of 1 cm where the FWHM is set to be 100 fs, 75 fs and 50 fs, respectively. When the pulse FWHM is reduced, the generated SC spectrum extends toward the mid-infrared region and large bandwidth spanning of 7.59 μm from 1.65 μm to 9.24 μm at 20 dB is successfully achieved when pumping with 50 fs FWHM pulses. The SC sensitivity to the input noise is, then, analyzed. The coherence of SC spectra generated in our proposed PCF is investigated by considering the optimized parameters of the input pulse. Figure 11 shows the SC generated after 1 cm of propagation in the PCF using a pulse with a peak power and FWHM of 20 kW and 50 fs, respectively and the corresponding first-order degree of coherence calculated from 100 independent realizations. As it can be seen, the generated spectrum exhibits smooth profile with perfect spectral coherence over the entire spectral range. In fact, the spectral broadening is achieved mainly due to SPM which is a deterministic process that preserves the coherence of input optical pulses [40]. Finally, the influence of the material loss on the SC spectral bandwidth is examined. Figure 12 depicts the output SC spectrum for a laser pulse with a peak power and FWHM of 20 kW and 50 fs, respectively, without loss and after introducing an optical attenuation with a coefficient of 1.24 dB/mm, calculated from the transmission spectra of the Ga-Sb-S glass system [23]. Compared to the case where the loss is neglected, the generated SC spectrum bandwidth at the spectral flatness level of 20 dB is reduced only by 0.29 μm. Besides, this spectral narrowing can be compensated by increasing the input pulses peak power.

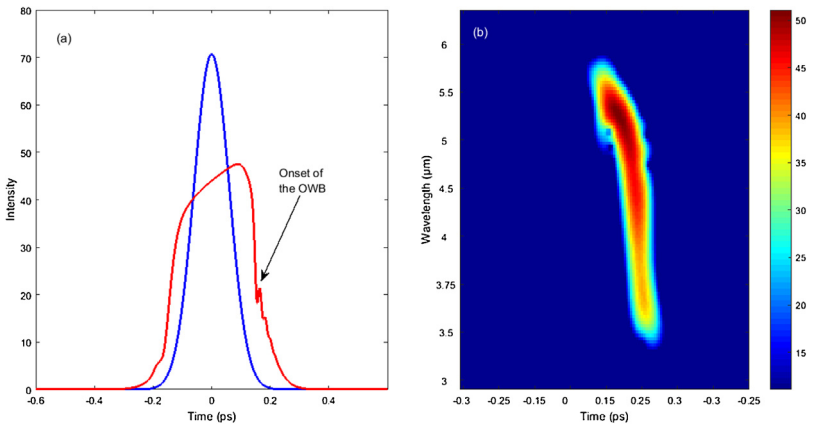

Fig. 8. (a) Pulse profiles at the input and after $z = 3.3$ mm of propagation. (b) Spectrogram of the output pulse.

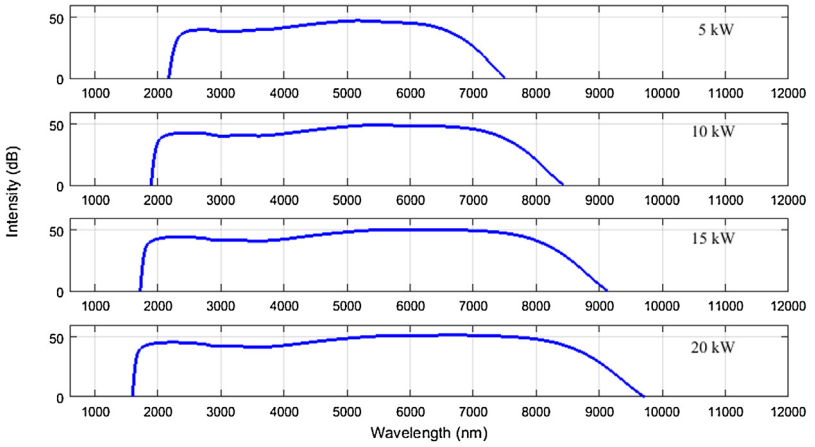

Fig. 9. Generated SC spectrum in 1 cm PCF length with an input pulse FWHM of 50 fs and various values of the peak power.

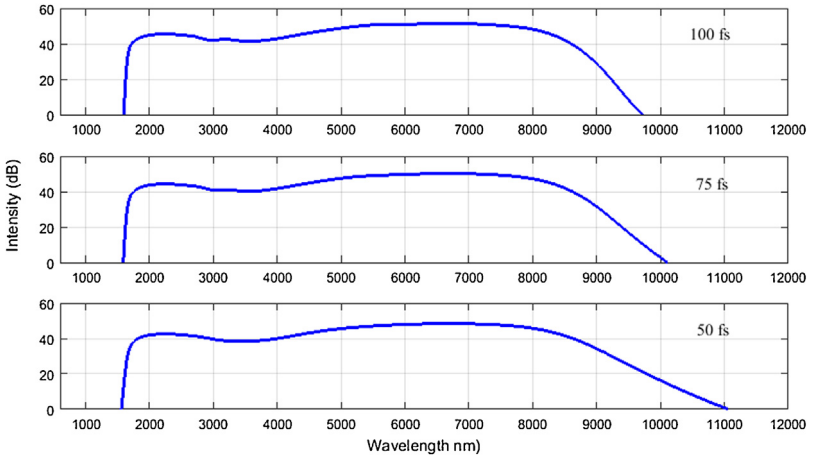

Fig. 10. Generated SC spectrum in 1 cm PCF length with an input pulse peak power of 20 kW and various values of FWHM.

The numerical results presented in this paper are compared to recently published works reporting mid-infrared SC generation in ANDi ChG based PCFs (Table 2). Although the comparison is performed by considering a spectral flatness of 20 dB level, it reveals the potential of our proposed $Ga_8Sb_{32}S_{60}$ ChG glass based PCF to generate coherent, broadband and ultra-flat SC spectra.

Also, it is worth noting that the SC is generated in our PCF with a simple design compared to more complex structures such as multi-material PCFs [19,22], PCF with different air holes diameters [17] or nanostructured graded-index fiber [43].

The broadband SC generated in our proposed $Ga_8Sb_{32}S_{60}$ glass PCF makes it a promising candidate for multiple nonlinear applications, especially in OCT [44]. Visible and near-infrared OCT has been widely used as non-invasive and non-contact cross-sectional imaging technique for biological tissues, material characterization, dimensional measurement etc. [45]. Recently, mid-infrared OCT systems have been reported for the analysis of ceramics, polymers

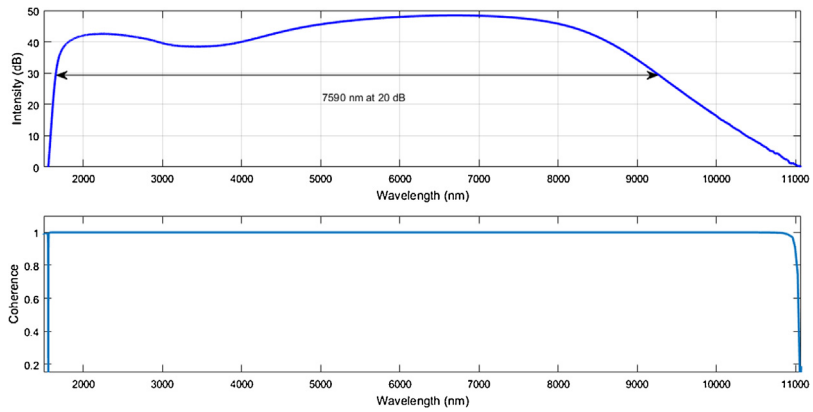

Fig. 11. SC generated with an input Gaussian pulse peak power and FWHM of 20 kW and 50 fs, respectively and the calculated degree of coherence.

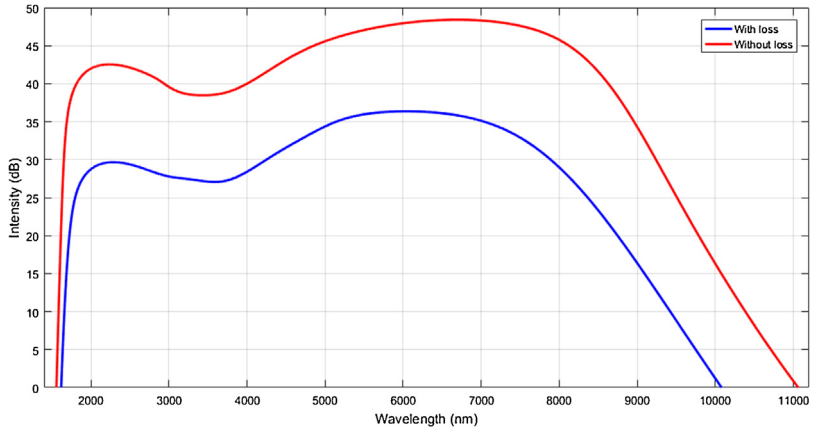

Fig. 12. SC generated with an input Gaussian pulse peak power and FWHM of 20 kW and 50 fs, respectively with and without introducing optical material loss.

Table 2
Comparison of the SC bandwidth at 20 dB generated with the proposed $Ga_8Sb_{32}S_{60}$ based PCF with that reported in selected ANDi ChG based PCF designs.'.

Reference	ChG glass	Pump wavelength (μm)	SC bandwidth (μm)
[17]	As_2Se_3	4.5	2 - 8
[18]	$As_{38.8}Se_{61.2}$	3.7	2.8 – 4.8
[19]	As_2S_5 – borosilicate	2.5	0.9 – 5.25
[21]	$Ge_{11.5}As_{24}Se_{64.5}$	3.1	2 - 5.5
[22]	$Ge_{11.5}As_{24}Se_{64.5}$ - $Ge_{11.5}As_{24}S_{64.5}$	4	2.5 - 7
[41]	As_2S_3 - borosilicate	2.8	2.4 – 3.1
[42]	As_2S_3	2.5	1-7.5
[43]	$As_{40}Se_{60}$ - $Ge_{10}As_{23.4}Se_{66.6}$	6.3	3.5 – 8.5
Proposed PCF	$Ga_8Sb_{32}S_{60}$	4.5	1.65 - 9.24

and some biochemical species such as collagen amide, carbonate and phosphate [46,47]. For an OCT system, an axial resolution is a key specification. Its value is determined by the coherence length of the light source given by [48]:

$$L_c = \frac{2\ln 2}{\pi}\frac{\lambda_0^2}{\Delta\lambda}. \tag{13}$$

Where λ_0 and $\Delta\lambda$ are the source center wavelength and spectral bandwidth, respectively. As it can be noticed from Eq. (13), the coherence length is inversely proportional to the optical source spectral bandwidth and, therefore, broadband optical sources are needed to design OCT systems with improved axial resolution [48]. In our simulations, we have found that pumping 1.06 nJ pulses at a central wavelength of 4.5 μm into a 1 cm long PCF generates a broad SC with the spectral width $\Delta\lambda = 7.59$ μm. Therefore, the coherence length is 1.18 μm and, hence, high resolution OCT imaging system can be ensured for the mid-infrared fingerprint region. Besides, the ultra-flatness of the generated SC prevents the creation of side lobes in the interferogram and ensures the required high quality of axial resolution [47].

Considering now the fabrication possibilities of the proposed PCF. A key factor for fiber manufacturing is related to the thermal stability of the host glass. Thermal stability is defined as the difference ΔT between the crystallization temperature T_c and the glass transition temperature T_g which has to be higher than 100^0 C [49,50]. According to the experimental results reported in [23], the glass transition and crystallization temperatures of the $Ga_8Sb_{32}S_{60}$ glass are found to be $T_g = 240^0$ C and $T_c = 357^0$ C, leading to a thermal stability of $\Delta T = T_g - T_c = 117^0$ C. For that reason, the $Ga_8Sb_{32}S_{60}$ chalcogenide glass system is found suited for fibers fabrication.

4. Conclusions

In summary, we have studied ANDi and highly nonlinear chalcogenide glass based PCF for coherent, broadband and flat-top mid-infrared SC generation. The proposed PCF consists of a solid

core made of $Ga_8Sb_{32}S_{60}$ ChG glass surrounded by seven rings of air holes arranged in a hexagonal lattice. Numerical results indicate that targeted dispersion properties can be achieved simply by controlling the air hole diameters in the cladding and ANDi profile is achieved over a wide range of wavelengths with a zero dispersion wavelength located around 4.5 μm. Moreover, the proposed PCF exhibits Kerr nonlinearity as high as 970 $w^{-1}\,km^{-1}$ at the pumping wavelength (i.e., 4.5 μm). Furthermore, SC generation at 4.5 μm in the optimized design has been analyzed. The impact of input pulse peak power and duration on output spectral bandwidth have been investigated. Simulations' results have shown that broadband and perfectly coherent flat-top SC spectrum spanning the wavelength range from 1.65 μm to 9.24 μm at the 20 dB spectral level is successfully generated by using a 50 fs duration 20 kW peak power laser pulse (corresponding to pulse energy of 1.06 nJ) in only 1 cm PCF length. Owing to its interesting properties, the proposed $Ga_8Sb_{32}S_{60}$ glass PCF is found to be suitable for potential mid-infrared applications such as optical coherence tomography, mid-infrared spectroscopy, metrology and material characterization.

CRediT authorship contribution statement

A. Medjouri: Conceptualization, Investigation, Writing - original draft, Writing - review & editing. **D. Abed:** Writing - original draft, Writing - review & editing. **Z. Becer:** Writing - original draft.

References

[1] R.R. Alfano, The Supercontinuum Laser Source: the Ultimate White Light, 3rd edition, Springer, 2016, http://dx.doi.org/10.1007/978-1-4939-3326-6.
[2] R.R. Alfano, S.L. Shapiro, Observation of self-phase modulation and small-scale filaments in crystals and glasses, Phys. Rev. Lett. 24 (1970) 592–596, http://dx.doi.org/10.1103/PhysRevLett.24.592.
[3] D. Faccio, J.M. Dudley, Frontiers in modern optics, in: Proceedings of the International School of Physics, Enrico Fermi, IOS Press, The Netherlands, 2016.
[4] J.M. Dudley, J.R. Taylor, Supercontinuum Generation in Optical Fibers, Cambridge University Press, 2010, http://dx.doi.org/10.1017/CBO9780511750465.
[5] J.M. Dudley, G. Genty, S. Coen, Supercontinuum generation in photonic crystal fiber, Rev. Mod. Phys. 78 (2006) 1135–1184, http://dx.doi.org/10.1103/RevModPhys.78.1135.
[6] A. Hartung, A.M. Heidt, H. Bartelt, Design of all-normal dispersion microstructured optical fibers for pulse-preserving supercontinuum generation, Opt. Express 19 (2011) 7742–7749, http://dx.doi.org/10.1364/OE.19.007742.
[7] A.M. Heidt, A. Hartung, G.W. Bosman, P. Krok, E.G. Rohwer, H. Schwoerer, H. Bartelt, Coherent octave spanning near-infrared and visible supercontinuum generation in all-normal dispersion photonic crystal fibers, Opt. Express 19 (2011) 3775–3787, http://dx.doi.org/10.1364/OE.19.003775.
[8] M. Yasin, Sulaiman Wadi Harun, H. Arof, Recent progress in optical fiber research, InTech (2012), http://dx.doi.org/10.5772/2428.
[9] R. Thomson, C. Leburn, D. Reid, Ultrafast Nonlinear Optics, Springer, 2013, http://dx.doi.org/10.1007/978-3-319-00017-6.
[10] L. Thévenaz, Advanced fiber optics concepts and technology, EPFL press, Switzerland, 2011.
[11] P. St.J. Russell, Photonic-crystal fibers, J. Lightwave Technol. 24 (12) (2006) 4729–4749, http://dx.doi.org/10.1109/JLT.2006.885258.
[12] A. Zakery, S.R. Elliot, Optical Nonlinearities in Chalcogenide Glasses and Their Applications, Springer, 2007, http://dx.doi.org/10.1007/978-3-540-71068-4.
[13] S. Wabnitz, B.J. Eggleton, All-optical Signal Processing: Data Communication and Storage Applications, Springer, 2015, http://dx.doi.org/10.1007/978-3-319-14992-9.
[14] N. Granzow, M.A. Schmidt, W. Chang, L. Wang, Q. Coulombier, J. Troles, P. Toupin, I. Hartl, K.F. Lee, M.E. Fermann, L. Wondraczek, P.St.J. Russell, Mid-infrared supercontinuum generation in As_2S_3-silica "nano-spike" step-index waveguide, Opt. Express 21 (2013) 10969–10977, http://dx.doi.org/10.1364/OE.21.010969.
[15] B.J. Eggleton, B.L. Davies, K. Richardson, Chalcogenide photonics, Nat. Photonics 5 (2011) 141–148, http://dx.doi.org/10.1038/nphoton.2011.309.
[16] P. Yan, R. Dong, G. Zhang, H. Li, S. Ruan, H. Wei, J. Luo, Numerical simulation on the coherent time-critical 2–5 mm supercontinuum generation in an As_2S_3 microstructured optical fiber with all-normal flat-top dispersion profile, Opt. Commun. 293 (2013) 133–138, http://dx.doi.org/10.1016/j.optcom.2012.11.093.
[17] T.S. Saini, A. Kumar, R.K. Sinha, Broadband mid-IR supercontinuum generation in As_2Se_3 based chalcogenide photonic crystal fiber: a new design and analysis, Opt. Commun. 345 (2015) 13–19, http://dx.doi.org/10.1016/j.optcom.2015.02.049.
[18] M. Diouf, A. Ben Salem, R. Cherif, H. Saghaei, A. Wague, Super-flat coherent supercontinuum source in $As_{38.8}Se_{61.2}$ chalcogenide photonic crystal fiber with all-normal dispersion engineering at a very low input energy, Pure Appl. Opt. J. Eur. Opt. Soc. Part A 56 (2) (2017) 163–169, http://dx.doi.org/10.1364/AO.56.000163.
[19] A. Ben Salem, M. Diouf, R. Cherif, A. Wague, M. Zghal, Ultraflat-top mid-infrared coherent broadband supercontinuum using all normal As_2S_5-borosilicate hybrid photonic crystal fiber, Opt. Eng. 55 (6) (2016), 066109, http://dx.doi.org/10.1117/1.OE.55.6.066109.
[20] M. Diouf, R. Cherif, A. Ben Salem, A. Wague, Ultra-broadband, coherent mid-IR supercontinuum expanding from 1.5 to 12.2 μm in new design of $AsSe_2$ photonic crystal fibre, J. Mod. Optic. 64 (13) (2017) 1335–1341, http://dx.doi.org/10.1080/09500340.2017.1288830.
[21] M.R. Karim, H. Ahmad, B.M.A. Rahman, All-normal dispersion chalcogenide PCF for ultraflat mid-infrared supercontinuum generation, IEEE Photonics Technol. Lett. 29 (21) (2017) 1792–1795, http://dx.doi.org/10.1109/LPT.2017.2752214.
[22] M.R. Karim, H. Ahmad, B.M.A. Rahman, Design and modeling of dispersion-engineered all-chalcogenide triangular-core fiber for mid infrared-region supercontinuum generation, J. Opt. Soc. Am. B 35 (2) (2018) 266–275, http://dx.doi.org/10.1364/JOSAB.35.000266.
[23] A. Yang, M. Zhang, L. Li, Y. Wang, B. Zhang, Z. Yang, D. Tang, Ga–Sb–S Chalcogenide Glasses for Mid-Infrared Applications, J. Am. Ceram. Soc. 99 (1) (2016) 12–15, http://dx.doi.org/10.1111/jace.14025.
[24] T.S. Saini, U.K. Tiwari, R.K. Sinha, Rib waveguide in Ga-Sb-S chalcogenide glass for on-chip mid-IR supercontinuum sources: design and analysis, J. Appl. Phys. 122 (2017), 053104, http://dx.doi.org/10.1063/1.4997541.
[25] J. Boruah, T.S. Saini, R.K. Sinha, Low bend loss photonic crystal fiber in Ga–Sb–S-based chalcogenide glass for nonlinear applications: design and analysis, J. Nanophotonics 11 (3) (2017), 036002, http://dx.doi.org/10.1117/1.JNP.11.036002.
[26] S. Guo, F. Wu, S. Albin, H. Tai, R.S. Rogowski, Loss and dispersion analysis of microstructured fibers by finite-difference method, Opt. Express 12 (2004) 3341–3352, http://dx.doi.org/10.1364/OPEX.12.003341.
[27] Z. Zhu, T.G. Brown, Full-vectorial finite-difference analysis of microstructured optical fibers, Opt. Express 10 (2002) 853–864, http://dx.doi.org/10.1364/OE.10.000853.
[28] A. Medjouri, L.M. Simohamed, O. Ziane, A. Boudrioua, Analysis of a new circular photonic crystal fiber with large mode area, Optik 126 (2015) 5718–5724, http://dx.doi.org/10.1016/j.ijleo.2015.09.035.
[29] G.P. Agrawal, Nonlinear Fiber Optics, 5th edition, Academic Press, 2013.
[30] K. Rottwitt, J.H. Povlsen, Analyzing the fundamental properties of Raman amplification in optical fibers, J. Lightwave Technol. 23 (2005) 3597–3605, http://dx.doi.org/10.1109/JLT.2005.857776.
[31] M. Klimczak, G. Soboń, R. Kasztelanic, K.M. Abramski, R. Buczyński, Direct comparison of shot-to-shot noise performance of all normal dispersion and anomalous dispersion supercontinuum pumped with sub-picosecond pulse fiber-based laser, Sci Rep-Uk 6 (2016) 1–14, http://dx.doi.org/10.1038/srep19284.
[32] G. Genty, A.T. Friberg, J. Turunen, Chapter two-Coherence of supercontinuum light, Prog. Optics 61 (2016), http://dx.doi.org/10.1016/bs.po.2015.10.002.
[33] M.H. Frosz, Validation of input-noise model for simulations of supercontinuum generation and rogue waves, Opt. Express 18 (2010) 14778–14787, http://dx.doi.org/10.1364/OE.18.014778.
[34] C. Ciret, S.P. Gorza, Generation of ultra-broadband coherent supercontinuum in tapered and dispersion managed silicon nanophotonic waveguides, J. Opt. Soc. Am. B 34 (2017) 1156–1162, http://dx.doi.org/10.1364/JOSAB.34.001156.
[35] M. Klimczak, B. Siwicki, A. Heidt, R. Buczyński, Coherent supercontinuum generation in soft glass photonic crystal fibers, Photonics Res 5 (6) (2017) 710–727, http://dx.doi.org/10.1364/PRJ.5.000710.
[36] R.W. Boyd, Nonlinear Optics, 3rd edition, Academic Press, 2008.
[37] R.A. Kaindl, M. Wurm, K. Reimann, P. Hamm, A.M. Weinerand, M. Woerner, Generation, shaping, and characterization of intense femtosecond pulses tunable from 3 to 20 μm, J. Opt. Soc. Am. B 17 (12) (2000) 2086–2094, http://dx.doi.org/10.1364/JOSAB.17.002086.
[38] W.J. Tomlinson, R.H. Stolen, A.M. Johnson, Optical wave breaking of pulses in nonlinear optical fibers, Opt. Lett. 10 (9) (1985) 457–459, http://dx.doi.org/10.1364/OL.10.000457.
[39] C. Finot, B. Kibler, L. Provost, S. Wabnitz, Beneficial impact of wave-breaking for coherent continuum formation in normally dispersive nonlinear fibers, J. Opt. Soc. Am. B 25 (2008) 1938–1948, http://dx.doi.org/10.1364/JOSAB.25.001938.
[40] L.E. Hooper, P.J. Mosley, A.C. Muir, W.J. Wadsworth, J.C. Knight, Coherent supercontinuum generation in photonic crystal fiber with all-normal group velocity dispersion, Opt. Express 19 (2011) 4902–4907, http://dx.doi.org/10.1364/OE.19.004902.
[41] P.S. Maji, P.R. Chaudhuri, Design of all-normal dispersion based on multimaterial photonic crystal fiber in IR region for broadband supercontinuum generation, Pure Appl. Opt. J. Eur. Opt. Soc. Part A 54 (13) (2015) 4042–4048, http://dx.doi.org/10.1364/AO.54.004042.

[42] M. Kalantari, A. Karimkhani, H. Saghaei, Ultra-Wide mid-IR supercontinuum generation in As_2S_3 photonic crystal fiber by rods filling technique, Optik 158 (2018) 142–151, http://dx.doi.org/10.1016/j.ijleo.2017.12.014.
[43] B. Siwicki, A. Filipkowski, A. Kasztelanic, A. Klimczak, A. Buczyński, Nanostructured graded-index core chalcogenide fiber with all-normal dispersion– design and nonlinear simulations, Opt. Express 25 (11) (2017) 12984–12998, http://dx.doi.org/10.1364/OE.25.012984.
[44] L. Froehly, J. Meteau, Supercontinuum sources in optical coherence tomography: A state of the art and the application to scan-free time domain correlation techniques and depth dependant dispersion compensation, Opt. Fiber Technol. 18 (2012) 411–419, http://dx.doi.org/10.1016/j.yofte.2012.08.001.
[45] R. Su, M. Kirillin, E.W. Chang, E. Sergeeva, S.H. Yun, L. Mattsson, Perspectives of mid-infrared optical coherence tomography for inspection and micrometrology of industrial ceramics, Opt. Express 22 (13) (2014) 15804–15819, http://dx.doi.org/10.1364/OE.22.015804.
[46] A.V. Paterova, H. Yang, C. An, D.A. Kalashnikov, L.A. Krivitsky, Tunable optical coherence tomography in the infrared range using visible photons, Quantum Sci. Technol. 3 (2018), 025008, http://dx.doi.org/10.1088/2058-9565/aab567.
[47] C.S. Colley, J.C. Hebden, D.T. Delpy, A.D. Cambrey, R.A. Brown, E.A. Zibik, W.H. Ng, L.R. Wilson, J.W. Cockburn, Mid-infrared optical coherence tomography, Rev. Sci. Instrum. 78 (2007), 123108, http://dx.doi.org/10.1063/1.2821609.
[48] W. Drexler, J.G. Fujimoto, Optical Coherence Tomography: Technology and Applications, Springer, 2015, http://dx.doi.org/10.1007/978-3-319-06419-2.
[49] H. Takebe, D.J. Brady, D.W. Hewak, K. Morinaga, Thermal properties of Ga_2S_3-based glass and their consideration during fiber drawing, J. Non-Cryst. Solids 258 (1-3) (1999) 239–243, http://dx.doi.org/10.1016/S0022-3093(99)00540-2.
[50] V.A.G. Rivera, D. Manzani, Technological Advances in Tellurite Glasses Properties, Processing, and Applications, Springer, 2017, http://dx.doi.org/10.1007/978-3-319-53038-3.